

行政院國家科學委員會補助專題研究計畫

成果報告  
 期中進度報告

以光感高分子材料製作垂直梳狀致動器(1/2)

計畫類別： 個別型計畫       整合型計畫

計畫編號：NSC 97 - 2221 - E - 009 - 021 - MY2

執行期間： 97 年 08 月 01 日至 99 年 07 月 31 日

計畫主持人：徐文祥

共同主持人：

計畫參與人員：鍾君煒、黃元德、王澤瑋、溫弘明

成果報告類型(依經費核定清單規定繳交)： 精簡報告       完整報告

本成果報告包括以下應繳交之附件：

- 赴國外出差或研習心得報告一份
- 赴大陸地區出差或研習心得報告一份
- 出席國際學術會議心得報告及發表之論文各一份
- 國際合作研究計畫國外研究報告書一份

處理方式：除產學合作研究計畫、提升產業技術及人才培育研究計畫、列管計畫及下列情形者外，得立即公開查詢

涉及專利或其他智慧財產權， 一年  二年後可公開查詢

執行單位：國立交通大學機械系

中 華 民 國      98 年      05 月      30 日

## 中文摘要：

垂直式梳狀致動器有優異的出平面運動特性，是最著名的微機電元件之一，以往多以矽作為其結構材料。相對於矽基材料，高分子材料處理屬低溫及低成本的製程，在僅需類 LIGA 製程基礎設備的狀況下，提供了高整合性以及容易負擔的製作方案。本計畫即是首先提出以光感高分子材料來製作垂直式梳狀致動器。

本研究團隊提出了一種雙面多重部分曝光(DoMPE)的製程平台，此平台經由正面及背面的多階曝光，可有效擴充懸浮光阻結構的外形複雜度。本年的重點在針對正型光阻，經由此平台建立的參數資料庫，對垂直式梳狀致動器進行製作、分析與實驗量測，成功驗證本構想之可行性，未來將持續拓展此平台技術至負型光阻。

關鍵詞：光阻、雙面、部份曝光、垂直梳狀致動器

## 英文摘要：

Vertical comb drives (VCDs) have attracted lots of attention due to their superior characteristics in out-of-plane motion. To date, all the reported VCDs were fabricated by silicon-based micromachining with silicon as the structural material. In contrast to silicon, polymer is an attractively alternative material for low-temperature process and low cost, which provides a flexible and affordable solution with the basic equipments in LIGA-like process. Here vertical comb drives made of polymers are proposed, fabricated, and tested.

A novel double-side multiple partial exposure (DoMPE) method is first developed to extend the multi-level morphology on both the front and back sides of the suspended photoresist microstructures. This year, through the established process parameters on positive photoresist, AZ9260, polymer VCDs are successfully fabricated, analyzed, and tested. The process parameters in DoMPE platform on negative photoresist, SU8, is on the way.

**Key words:** photoresist, double side, partial exposure, vertical comb drive

## 1. 前言

As a well known component, the electrostatic comb drive has rapidly occupied an important position in micro electromechanical systems (MEMS) technology since the first report by Tang *et al.* [1]. With two sets of fingers, the comb drive provides a constant output force and good linearity on capacitive sensing over a considerable displacement range because of the constant gap between the stationary finger and movable finger during the operation. Therefore, the comb drive has been widely investigated, such as the optimal shape design [2] and the sub-micron gap comb drive [3], and employed for MEMS applications, such as the filter [4], accelerometer [5], gyroscope [6], and optical switch [7].

In addition to the operation in the in-plane direction, the comb drive has also been fabricated with two sets of fingers owning a vertical offset to cause the out-of-plane motion, which is called the vertical comb drive (VCD). Comparing to the parallel plate electrostatic actuator, the VCD ideally generates the steady force over its entire stroke under one applied voltage, and exhibits no pull-in effect. Therefore, the VCDs are very suitable for the applications requiring the large out-of-plane displacement, low driving voltage, low power consumption, and high operation speed. For these superior characteristics, lots of investigations on the VCDs have been reported in the recent decade [8-19]. In these literatures, the fabrication methods could be divided into two categories. The first approach fabricated two sets of fingers owing a natural offset, such as the SUMMiT-V process [8], the polysilicon refilled and bulk etching [9], the bonding method [10], the SOI-based technique combining the DRIE etching [11-13], the multiple DRIE etching on single-crystal silicon substrate [14] and the micromachining on (111) single-crystal silicon substrate [15-16]. The second approach used the deforming mechanism to elevate or degrade one set of the comb fingers to create the required initial offset, such as the bending beam caused by residual stress [17], the photoresist reflowing [18], and the plastic deformation [19]. All these above mentioned methods used the single-crystal silicon or polysilicon as the structural materials.

In contrast to the silicon-based materials, the polymer has become another attractive material in the MEMS technology recently because of their relatively low cost and much easier processing steps. For example, the polycarbonate (PC) and polymethylmetacrylate (PMMA) have been utilized to fabricate the high aspect ratio microstructures by hot embossing method for MEMS applications [20]. The micro fluidic devices for micro total analysis systems ( $\mu$ -TAS) applications were also widely fabricated by PMMA, PC, polypropylene (PP), and polydimethylsiloxane (PDMS), etc. [21-23]. In addition to the passive components, the active micro devices have also been demonstrated by polymer materials to lower the cost, such as the electrostatic comb drive constructed by PMMA via the hot embossing technique [24], or by the thick negative photoresist SU-8 [25]. The accelerometer has also been fabricated by using SU-8 as the structural material [26], and the polymer micromechanical devices coated by metal layer via the electroless deposition technique have also been demonstrated [27]. Therefore, polymer is becoming a greatly important low cost alternative to their silicon or glass-based counterparts. However, no vertical comb drive made of polymer material has been reported yet.

Here, a novel approach to fabricate the polymer torsional vertical comb drive is proposed. Without any additional sacrificial layer, the proposed double-side partial exposure method is applied to the positive thick photoresist AZ9260® to carve out the suspending upper fingers and the fixed lower fingers. With the proper overhang design to realize the electric isolation, the metal layer deposited on the structural surface by

sputtering provides a suitable electric conductivity. This approach provides a simple, flexible, and low cost solution to fabricate the polymer VCDs.

## 2. 原理與分析

As the schematic illustration shown in figure 1, the torsional vertical comb drive (VCD) demonstrated in this paper consists of two sets of comb fingers. One set of fingers is fixed on the substrate, and the other set of fingers is suspended and connected to the suspending plate which is supported by the anchors through the torsion springs. With the voltage applied between the upper and lower fingers, the VCD could be driven into torsional motion by the electrostatic force until it is balanced by the mechanical force of the torsion springs. By solving the force balance equation, the relationship of driving voltage and torsion angle could be determined.

### 2.1 Electrostatic Force

In general, the electrostatic force per unit length generated by the comb drive with  $n$  finger pairs is given by

$$F_e(z) = \frac{n}{2} \frac{dC}{dz} V^2 \quad (1)$$

where  $C$  is the capacitance per unit length between a single pair of fingers,  $z$  is the vertical displacement in the out-of-plane direction, and  $V$  is the applied voltage. However, the capacitance  $C$  could not be considered as a simple parallel plate assumption with the fringing fields due to the limited height (or thickness) of fingers. To characterize the  $dC/dz$  relationship, the finite element method (FEM) through software ANSYS is used to simulate the capacitance of single pair fingers at different displacements,  $z$ . Then, the twelfth-order polynomial curve fitting is performed to obtain the capacitance  $C$  as a function of displacement,  $z$ , which is expressed as

$$C(z) = a_{12}z^{12} + a_{11}z^{11} + a_{10}z^{10} + \dots + a_2z^2 + a_1z + a_0 \quad (2)$$

As illustrated in figure 2(a), in addition to the case without considering a electrically conductive substrate, so-called the bottom plate, the condition of lower fingers with conductive bottom plate is also analyzed. Figure 2(b) shows one example of the simulation and fitting results with the finger height of 35  $\mu\text{m}$ , the finger width of 14  $\mu\text{m}$ , and the gap of 4  $\mu\text{m}$ . The fitting curve agrees well with the simulation data. For the fingers with conductive bottom plate, the capacitance is similar to that without conductive bottom plate at initial 2/3 stroke, but quite different in the final part of stroke.

### 2.2 Force Balance Analysis

As illustrated by figure 3, the torque induced by the electrostatic force of VCD could be expressed as

$$T_e = \int_{x1}^{x2} F_e(z) L_r dx \quad (3)$$

where  $x1$  and  $x2$  indicate the overlap region of the upper and lower fingers along the suspending plate ( $x$  direction), and  $L_r$  is the moment arm of the electrostatic force  $F_e(z)$  about the torsional axis and

equating  $x \cos \theta$ , in which  $\theta$  is the rotation angle of the VCD. Because the vertical displacement  $z$  could be expressed as  $x \sin \theta$ , equation (3) could be re-written as

$$T_e(\theta) = \frac{nV^2 \cos \theta}{2} \left[ \sum_{k=1}^{12} \frac{k(a_k x^{k+1} \sin^{k-1} \theta)}{k+1} \right]_{x1}^{x2} \quad (4)$$

Equation (4) describes the torque induced by the electrostatic force under different rotation angle for a given voltage. In addition, the torque generated by the mechanical force of the torsion springs could be described by

$$T_m(\theta) = -\frac{G\theta(b^3 h + bh^3)}{6L} \quad (5)$$

where  $G$  is the shear modulus of elasticity;  $b$ ,  $h$  and  $L$  are the width, height and length of the torsion springs, respectively. By equations (4) and (5), the rotation angle of VCD could be found.

### 3. 製作

For the positive photoresist, only the photoresist suffering the exposure dosage over the threshold value will be removed during the development, so the freestanding microstructures can be achieved by patterning the photoresist from the back side via the dosage control. Here, a novel process using partial exposure method in both front and back sides is employed to fabricate the polymer-based torsional vertical comb drive and needs only three masks in total.

Figure 4 shows the detailed fabrication procedure of the proposed polymer VCD. The soda-lime glass is used as the substrate, and the commercial positive thick photoresist, AZ9260® (Clariant), is utilized to demonstrate this process. First, the Ti layer of 2500 Å is deposited and patterned by the lift-off process as the mask for the backside partial exposure, as shown in figure 4(a). Then, the photoresist AZ9260® with thickness about 55 μm is spin-coated and soft-baked at 90°C for 90 minutes, as shown in figure 4(b). After re-hydration, the photoresist is exposed by the front-side partial exposure for the desired development depths, as shown in figure 4(c), which defines the height, i.e. thickness, of the lower fingers. Then, the backside partial exposure is carried out for the suspending space of the upper fingers, as shown in figure 4(d), which provides the desired operation stroke of VCD. Subsequently, the full exposure is carried out to define the overall structure, as shown in figure 4(e), in which the upper and lower fingers are self-aligned to avoid the misalignment problem. After all the required exposing procedure, the final development is performed with the developer of AZ400k (20% diluted by de-ionized water). At this step, the release process of VCD is also completed without any additional sacrificial layer and etching step. Then, the structure of VCD is fabricated, as shown in figure 4(f), where the overhang design at the anchors is employed by defining a narrower width at the lower part of the anchors. Finally, in order to provide the desired electric conductivity to activate the VCD, a thin Cu layer with thickness of 2000 Å is deposited on the structural surface by sputtering system, and the overhang design can achieve electric isolation around undercut of the anchors to avoid the electric short between the upper and lower sets of fingers, as shown in figure 4(g).

### 4. 結果與討論

In this section, the parameters of photoresist processing are experimentally characterized first for the

reliable fabrication of vertical comb drive (VCD). Then, the fabrication results of polymer torsional VCDs by the proposed process are shown and discussed. Finally, the static and dynamic responses of VCD are measured and compared with the simulation results.

#### 4.1 Photoresist Processing

In general, the development depth of photoresist is mainly controlled by the exposure dosage. In other words, the larger dosage creates the deeper depth. However, other processing parameters of photoresist, such as the development time and soft-bake time, also play important roles in this process. In addition to the increase of exposure dosage, the longer development time will also enlarge the development depth of photoresist, but this enlargement could be evidently reduced by the longer soft-bake time. Therefore, a proper set of parameters is needed to obtain the stable fabrication results. Here, the photoresist thickness about 55  $\mu\text{m}$ , the soft-bake time of 90 minutes and the development time of 45 minutes are employed on the fabrication of polymer VCDs. With these parameters, figure 5 shows the development depths of AZ9260® under different exposure dosages. The results reveal that the development depth increases stably with the increasing exposure dosage. Depending on these experimental data, the desired suspending space of upper fingers and the height of lower fingers could be fabricated by using the corresponding dosages.

#### 4.2 Fabrication Results

With photoresist processing conditions described above, the polymer VCDs with two levels both in front and back sides are fabricated by the proposed process. Figure 6(a) shows the fabricated VCD made of AZ9260® after the final deposition of Cu by sputtering, where the size of suspending plate is  $300\mu\text{m}\times 360\mu\text{m}$ , and the width and length of torsion springs are 4  $\mu\text{m}$  and 60  $\mu\text{m}$ , respectively. A narrower or thinner torsion bar may reduce torsion spring constant for larger rotation angle, however, a thinner torsion spring will reduce the vertical rigidity more evidently, which may induce a larger vertical deflection of torsion spring to reduce effective rotation angle. Therefore a narrow torsion spring would be a feasible approach. However, stiction problem limits us to further reduce the width of torsion spring, since the surface tension in developing will pull down the suspended plate and even break the torsion spring without sufficient vertical rigidity.

The finger is 100  $\mu\text{m}$  long, 5  $\mu\text{m}$  wide, and the overlap length between fixed and movable fingers is around 80  $\mu\text{m}$ . The applied partial exposure dosage of  $426\text{ mJ/cm}^2$  creates the development depth about 20  $\mu\text{m}$  in the front-side direction, which results in the height of lower fingers about 35  $\mu\text{m}$ . By introducing partial exposure dosage of  $525\text{ mJ/cm}^2$  in the backside direction, the suspending space of upper fingers about 24  $\mu\text{m}$  is obtained, which indicates that the overlap depth between fixed and movable finger is 11  $\mu\text{m}$ , and the thickness of suspended structures is about 31  $\mu\text{m}$ . It is found that higher exposure dosage will enlarge the trench width and limit the minimum gap size to 8  $\mu\text{m}$  in our case. Figures 6(b) and 6(c) show the closed view and top view of the finger structures, respectively. Finally, the supporting bars near the upper fingers to avoid stiction are removed by the probe manually for the following measurements.

#### 4.3 Measurement and Comparison

The static deflection and dynamic responses of the polymer torsional VCD are measured in open air by

the white light interferometer and the MEMS motion analyzer (MMA), respectively. In measuring the rotation angle, the surface profiles of VCD at steady state under different driving voltages are first determined by the white light interferometer. Then the rotation angle can be calculated by the relative deflection between two reference points, such as the movable finger tip and the torsion spring. For vibration measurement, a sinusoid wave is applied to the VCD with frequency range from 1KHz to 10kHz, then the amplitude is recorded. By selecting the proper location, the dynamic responses at different frequencies can be obtained directly.

According to the measurement on static deflection, the maximum rotation angle of  $2.31^\circ$  can be achieved by the driving voltage of 158.3V with the same designed dimensions shown in figure 6. Figure 7 shows the measured results of dynamic response, where the VCD is activated by a sinusoid wave with amplitude of 20 V and an offset of 20 V, and the first-mode natural frequency of 6.6 kHz is obtained. With this characterized natural frequency, the elastic modulus could be found by further determining the density of photoresist. Here, a simple experiment is performed to obtain the density of AZ9260®. The photoresist is spin-coated on a wafer with the calibrated weight, and then patterned into a circle with a specified diameter. By determining the increase of total weight and the final thickness of photoresist film, the density of photoresist could be obtained through the characterized value of weight over volume. Then, with the determined density of  $1180 \pm 7 \text{ Kg/m}^3$  and first natural frequency of 6.6 kHz, the effective elastic modulus of 1.142 GPa is used in the FEM simulation, where the Poisson's ratio is assumed as 0.4. Figure 8 shows the simulated results of modal analysis, in which the model of the VCD includes the suspending plate, the torsion springs, and the upper fingers. The second, third, and fourth natural frequencies are also found as 41.40 kHz, 44.10 kHz, and 54.02 kHz, respectively.

With the above material properties, the static deflection of polymer VCD is calculated by the software Matlab through the analytical model described in section 2. Figure 9 shows the experimental and analytical results of the polymer torsional VCD, where the latter includes the cases with and without considering the conductive bottom plate. In the analytical results, the case without bottom plate electrodes presents a more linear behavior but a little smaller rotation angle under different driving voltages. For the case with conductive bottom plate, a similar behavior is observed in the first half stroke but there is a pull-in effect at the rotation angle of  $2.17^\circ$  with the applied voltage of 167.37V due to the obvious increase of the capacitance which induces the rapid rise of electrostatic force. By comparing to experimental results, where a snapping phenomenon is also observed between the voltages of 158.3V and 161.8V, the bottom plate effect has an evident influence on the performance of VCD, especially at high driving voltage. Furthermore, according to our simulations, it is found that the metal layer on the upper finger bottom has little effect on the rotation angle, since the width of the upper finger,  $5 \mu\text{m}$ , is much smaller than its height,  $31 \mu\text{m}$ . For example, when the driving voltage is 160 V, the rotation angle will change only from 1.804 degrees (metal layer on the upper finger bottom) to 1.792 degrees (without metal layer on the upper finger bottom).

The internal stress may also affect the performance of the torsional VCD. The residual gradient strain will result in curved surface, which would lift the movable fingers up to have an extra offset and reduce the overlap area. However, the torsional VCD with a larger offset can provide a longer stroke to allow larger rotation angle. In our case, the extra offset between movable finger center and fixed finger center due to the internal stress is found to be around  $3 \mu\text{m}$  initially, which is not considered in the simulation model. This

might be the reason why experimental results show larger rotation angles around 150 V than simulation results.

## 5. 結論

This investigation proposes a reliable approach to fabricate the polymer-based torsional vertical comb drive by using the positive thick photoresist AZ9260® as the structural material. A double-side partial exposure method is employed to create the suspending upper fingers and the fixed lower fingers without any additional sacrificial layer and etching process. The proper processing parameters of photoresist for the fabrication of polymer torsional VCDs have been established. For the activation of the polymer VCDs, the metal layer deposited on the structural surface by the sputtering system provides the desired electric conductivity while the overhang design realizes the electric isolation. According to the measurement results, the rotation angle of 2.31° can be achieved by the driving voltage of 158.3V, which agrees with the analytical results and verifies the feasibility of the proposed approach to fabricate the polymer VCDs. However, even the Young's modulus (1.142GPa) of AZ9260 covered by thin Cu layer is much lower than single crystal silicon (160~200GPa), comparing to torsional VCDs made of single crystal silicon reported previously [28, 29], the polymer torsional VCD fabricated here needs higher driving voltage to achieve the same rotation angle due to our limitations on fabrication capability. For example, the minimum gap size here is 8 μm, which could be further improved by a better exposure system. Another issue would be the thickness of the polymer. A thicker photoresist will be helpful to provide larger overlap area between fixed and movable fingers, also it may support larger suspended space to avoid stiction without using supporting bars.

## References

- [1] Tang W C, Nguyen T H and Howe R T 1998 Laterally driven polysilicon resonant microstructures *Tech. Dig. IEEE Micro Electro Mech. Syst. Workshop (Salt Lake City)* pp 53–9
- [2] Ye W, Mukherjee S and MacDonald N C 1998 Optimal shape design of an electrostatic comb drive in microelectromechanical systems *J. Microelectromech. Syst.* **7** 16–26
- [3] Hirano T, Furuhashi T, Gabriel K J and Fujita H 1992 Design, fabrication, and operation of submicron gap comb-drive microactuators *J. Microelectromech. Syst.* **1** 52–9
- [4] Lin L, Howe R T and Pisano A P 1998 Microelectromechanical filters for signal processing *J. Microelectromech. Syst.* **7** 286–94
- [5] Park K Y, Lee W C, Jang H S, Oh Y S and Ha B J 1998 Capacitive sensing type surface micromachined silicon accelerometer with a stiffness tuning capability *Dig. IEEE/ASME MEMS Workshop (Heidelberg, Germany)* pp 637–42
- [6] Tanaka K, Mochida Y, Sugimoto M, Moriya K, Hasegawa T, Atsuchi K and Ohwada K 1995 A micromachined vibrating gyroscope *Sensors and Actuators A* **50** 111–5
- [7] Juan W -H and Pang S W 1998 High-aspect-ratio Si vertical micromirror arrays for optical switching *J. Microelectromech. Syst.* **7** 207–13
- [8] Hah D, Huang S T -Y, Tsai J -C, Toshiyoshi H and Wu M C 2004 Low-voltage, large-scan angle MEMS analog micromirror arrays with hidden vertical comb-drive actuators *J. Microelectromech. Syst.* **13** 279–89

- [9] Selvakumar A and Najafi K 2003 Vertical comb array microactuators *J. Microelectromech. Syst.* **12** 440–9
- [10] Lee J -H, Ko Y -C, Kong D -H, Kim J -M, Lee K B and Jeon D -Y 2002 Design and fabrication of scanning mirror for laser display *Sensors and Actuators A* **96** 223–30
- [11] Yeh J -L A, Jiang H and Tien N C 1999 Integrated polysilicon and DRIE bulk silicon micromachining for an electrostatic torsional actuator *J. Microelectromech. Syst.* **8** 456–65
- [12] Hah D, Choi C -A, Kim C -K and Jun C -H 2004 A self-aligned vertical comb-drive actuator on an SOI wafer for a 2D scanning micromirror *J. Micromech. Microeng.* **14** 1148–56
- [13] Milanović V 2004 Multilevel beam SOI-MEMS fabrication and applications *J. Microelectromech. Syst.* **13** 19–30
- [14] Zhang Q X, Liu A Q, Li J and Yu A B 2005 Fabrication technique for microelectromechanical systems vertical comb-drive actuators on a monolithic silicon substrate *J. Vac. Sci. Technol. B* **23** 32–41
- [15] Kim J, Park S and Cho D 2001 A novel electrostatic vertical actuator fabricated in one homogeneous silicon wafer using extended SBM technology *Transducers '01* pp 756-9
- [16] Tsai J M -L, Chu H -Y, Hsieh J and Fang W 2004 The BELST II process for a silicon high-aspect-ratio micromachining vertical comb actuator and its applications *J. Micromech. Microeng.* **14** 235–41
- [17] Jeong K -H and Lee L P 2005 A novel microfabrication of a self-aligned vertical comb drive on a single SOI wafer for optical MEMS applications *J. Micromech. Microeng.* **15** 277–81
- [18] Hah D, Patterson P R, Nguyen H D, Toshiyoshi H and Wu M C 2004 Theory and experiments of angular vertical comb-drive actuators for scanning micromirrors *J. Selected Topics In Quantum Electronics* **10** 505–13
- [19] Kim J, Choo H, Lin L and Muller R S 2003 Microfabricated torsional actuator using self-aligned plastic deformation *Transducers '03* pp 1015–8
- [20] Becker H and Heim U 2000 Hot embossing as a method for the fabrication of polymer high aspect ratio structures *Sensors and Actuators A* **83** 130–5
- [21] Lee G -B, Chen S -H, Huang G -R, Sung W -C and Lin Y -H 2001 Microfabricated plastic chips by hot embossing methods and their applications for DNA separation and detection *Sensors and Actuators B* **75** 142–8
- [22] Becker H and Gärtner C 2000 Polymer microfabrication methods for microfluidic analytical applications *Electrophoresis* **21** 12–26
- [23] Abgrall P 2007 Lab-on-chip technologies: making a microfluidic network and coupling it into a complete microsystem—a review *J. Micromech. Microeng.* **17** R15–49
- [24] Zhao Y and Cui T 2003 Fabrication of high-aspect-ratio polymer-based electrostatic comb drives using the hot embossing technique *J. Micromech. Microeng.* **13** 430–5
- [25] Dai W, Lian K and Wang W 2007 Design and fabrication of a SU-8 based electrostatic microactuator *Microsyst. Technol.* **13** 271–7
- [26] Jeong S J and Wang W 2004 Microaccelerometers using cured SU-8 as structural material *Proc. SPIE* **5344** 115–23
- [27] Eberhardt W, Gerhäuser Th, Giousouf M, Kück H, Mohr R and Warkentin D 2002 Innovative concept for the fabrication of micromechanical sensor and actuator devices using selectively metallized

polymers *Sensors and Actuators A* **97–98** 473–7

- [28] Tsai J M-L, Chu H-Y, Hsieh J, and Fang W 2004 The BELST II process for a silicon high-aspect-ratio micromaching vertical comb actuator and its applications *J. Micromech. Microeng.* **14** 235–241
- [29] Jeong K-H, and Lee L P 2005 A novel microfabrication of a self-aligned vertical comb drive on a single SOI wafer for optical MEMS applications *J. Micromech. Microeng.* **15** 277–281

6. 圖表

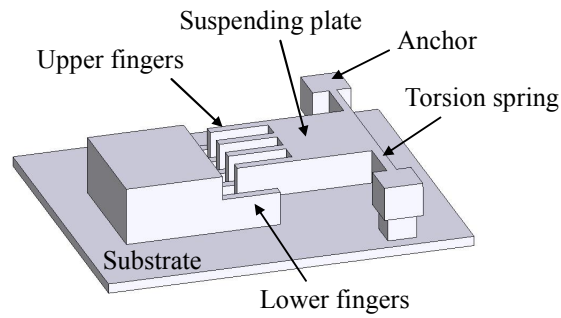


Figure 1. The schematic illustration of the torsional vertical comb drive.

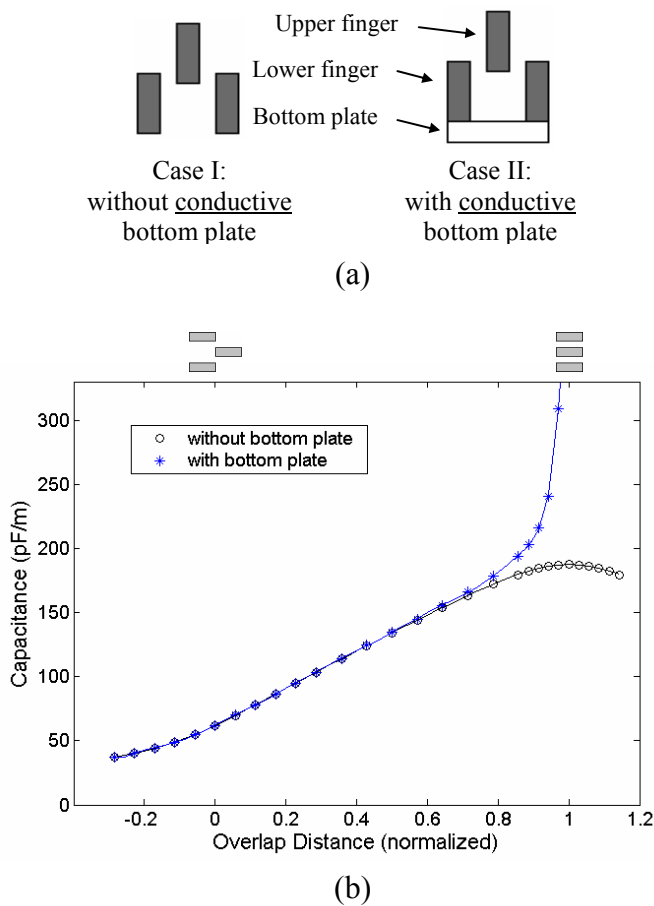


Figure 2. The simulated cases and results; (a) two simulated cases: with/without the conductive bottom plate; (b) the simulated capacitance of single pair fingers at different displacement  $z$  and the curve fitting results; the overlap distance is normalized by the finger height of  $35 \mu\text{m}$ .

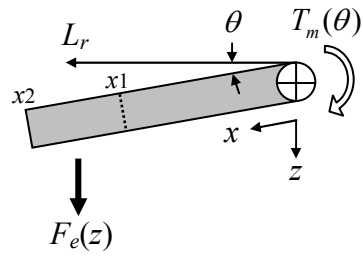


Figure 3. The illustration of the torque induced by electrostatic force from side view of the upper finger and suspending plate, where  $T_m(\theta)$  is the induced torque by the mechanical force of the torsion springs.

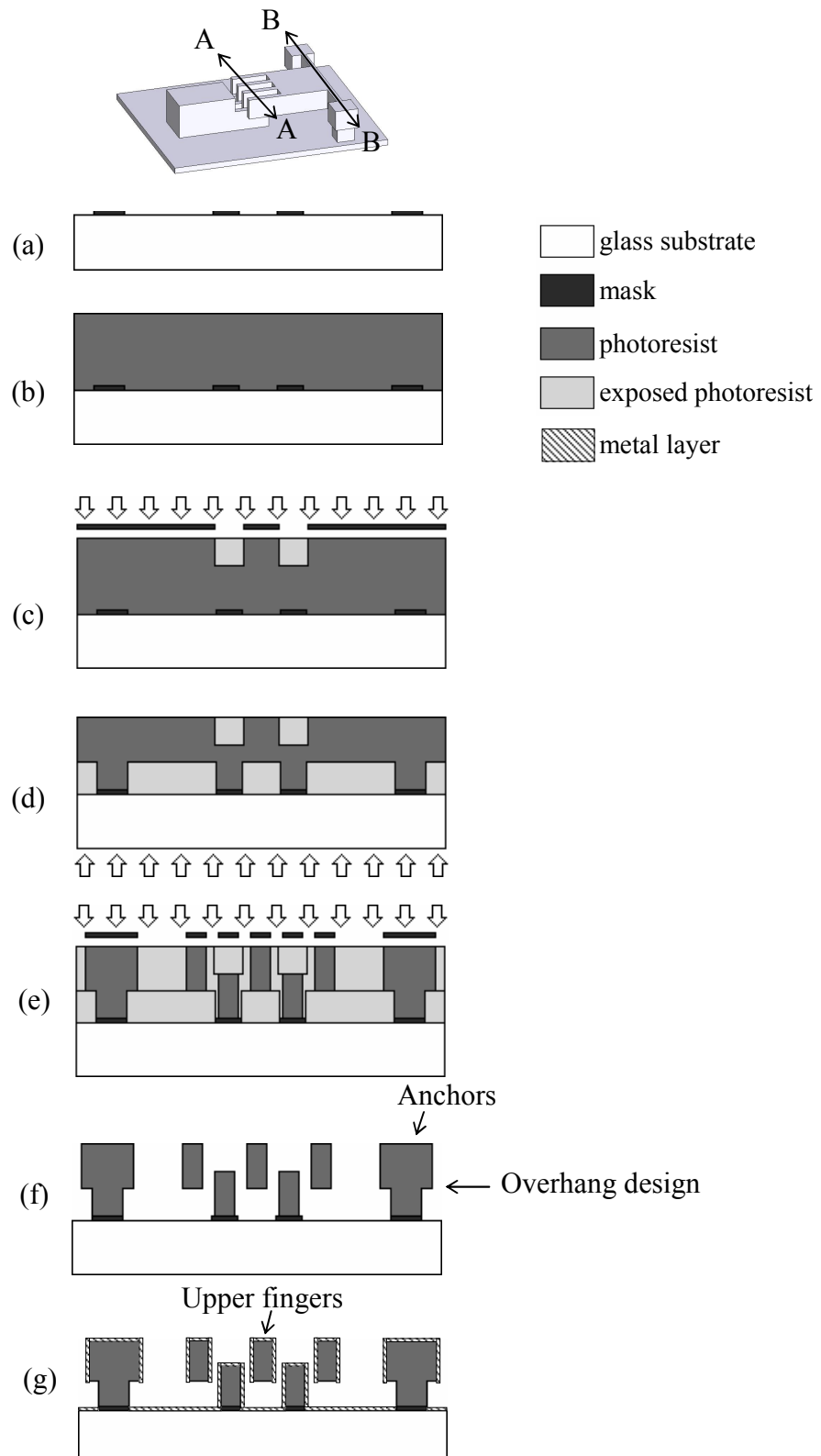


Figure 4. The fabrication process of the polymer VCD on the AA cross-section for fingers, and BB cross-section for anchors; (a) defining the Ti film as the backside mask; (b) coating the thick positive photoresist; (c) the front-side partial exposure; (d) the backside partial exposure; (e) the full exposure to define the overall structure; (f) development and release with overhanging design on anchors; (g) sputtering the Cu layer with electric isolation on anchor.

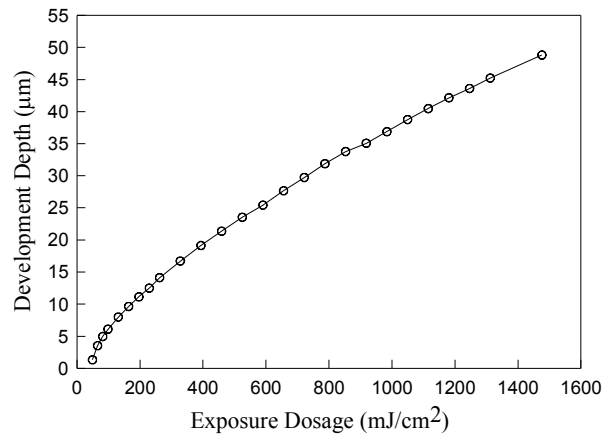
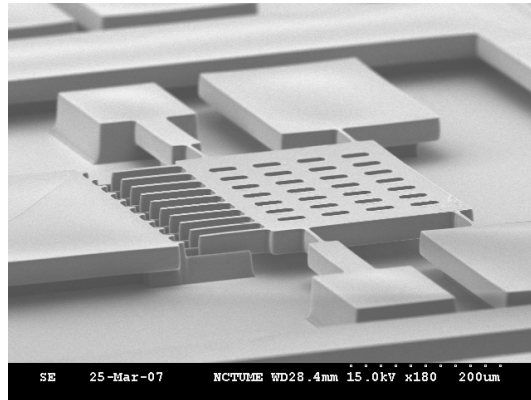
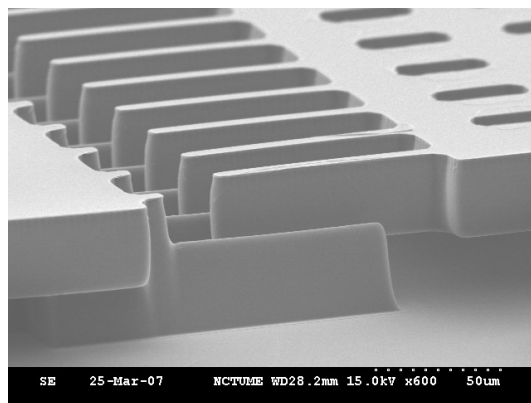


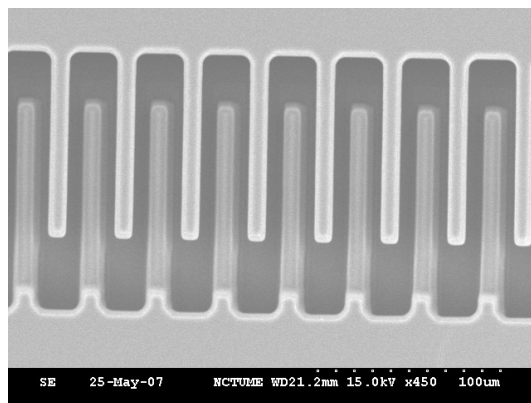
Figure 5. The relationship between the development depth and the exposure dosage of the photoresist AZ9260®.



(a)



(b)



(c)

Figure 6. The fabricated polymer torsional vertical comb drive by the double-side partial exposure method; (a) the over view of VCD; (b) the closed view and (c) top view of the finger structures.

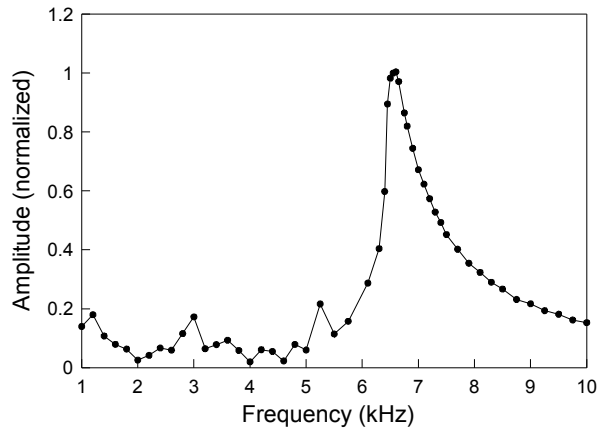


Figure 7. The dynamic response of torsional vertical comb drive; the peak response is obtained at 6.6 kHz.

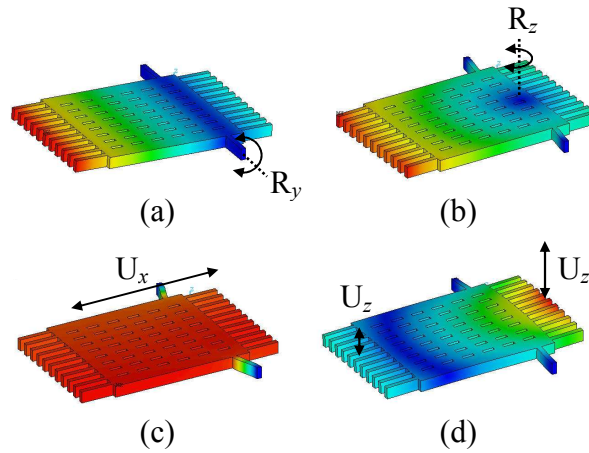


Figure 8. The mode shapes and natural frequencies of the vertical comb drive; (a)  $f_1=6.60$  kHz, (b)  $f_2=41.40$  kHz, (c)  $f_3=44.10$  kHz, and (d)  $f_4=54.02$  kHz.

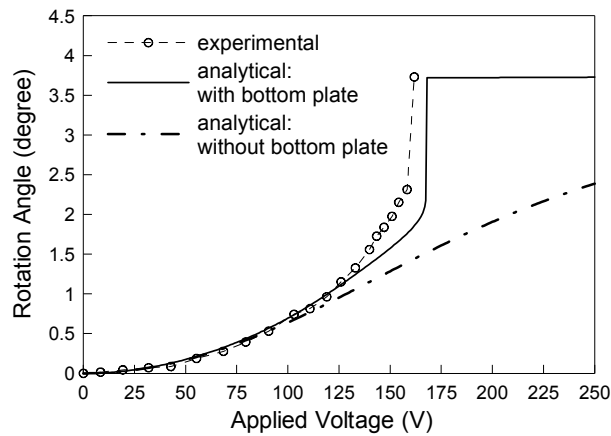


Figure 9. The experimental and analytical results of the static deflection of vertical comb drive, where the analytical results include the cases with and without conductive bottom plate.